Published in final edited form as:
Nat Clim Chang. 2021 ; 11: 449–455. doi:10.1038/s41558-021-01034-5.

Woody-biomass projections and drivers of change in sub-Saharan Africa

C. Wade Ross[1,2], **Niall P. Hanan**[1], **Lara Prihodko**[3], **Julius Anchang**[1], **Wenjie Ji**[1], **Qiuyan Yu**[1]

[1]Department of Plant and Environmental Sciences New Mexico State University, Las Cruces, NM, USA.

[2]Tall Timbers Research Station, Tallahassee, Florida 32312, USA.

[3]Animal and Range Sciences, New Mexico State University, Las Cruces, NM, USA.

Abstract

Africa's ecosystems have an important role in global carbon dynamics, yet consensus is lacking regarding the amount of carbon stored in woody vegetation and the potential impacts to carbon storage in response to changes in climate, land use, and other Anthropocene risks. Here, we explore the socio-environmental conditions that shaped the contemporary distribution of woody vegetation across sub-Saharan Africa and evaluate ecosystem response to multiple scenarios of climate change, anthropogenic pressures, and fire disturbance. Our projections suggest climate change will have a small but negative effect on above ground woody biomass at the continental scale, and the compounding effects of population growth, increasing human pressures, and socio-climatic driven changes in fire behavior further exacerbate climate-driven trends. Relatively modest continental-scale trends obscure much larger regional perturbations, with climatic and anthropogenic factors leading to increased carbon storage potential in East Africa, offset by large deficits in West, Central, and Southern Africa.

Planetary-scale consumption of resources, driven by rapid population and economic growth, has substantially increased emissions of CO_2 and other greenhouse gases[1,2]. Building on previous treaties, the Paris Agreement[3] developed international policy in an effort to limit global warming to less than 2°C above pre-industrial levels via decarbonization of energy systems and increased mitigation efforts, including improved land management

Correspondence: Correspondence and requests for materials should be addressed to C.W.R.

Author contributions
Funding acquisition: N.P.H, L.P.
Conceptualization: C.W.R., N.P.H., L.P.
Data assimilation, analysis, and visualizations: C.W.R.
Writing, reviewing, and editing: C.W.R., N.P.H., L.P., W.J., Q.Y., and J.A.

Data availability
This analysis was using the R programming language and ArcGIS. R code is available for download from Figshare at the following DOI: "https://doi.org/10.6084/m9.figshare.14143799.v1". Gridded projection maps are available for download at "https://doi.org/10.6084/m9.figshare.14150210.v2".

Competing interests
The authors declare no competing interests.

and ecosystem restoration to increase the carbon sink and storage capacity of terrestrial ecosystems. Achieving ambitious climate mitigation goals requires credible, accurate, and reliable mapping and monitoring of terrestrial carbon stock. As the second largest landmass, Africa's forests, woodlands, and savannas have a substantial impact on the global carbon budget by actively cycling carbon between the atmosphere, vegetation, and soil. However, the continent remains one of the largest sources of uncertainty in the global carbon cycle, functioning as both a sink and a source of CO_2 in response to natural and anthropogenic perturbations[4–9]. In recent decades, for example, severe droughts have impacted many humid and sub-humid regions[10,11], leading to tree mortality and loss of biomass[12]. Conversely, several studies have reported the recovery of African drylands following severe droughts of the 1970s and 1980s, attributed to post-drought vegetation recovery. Improvements in land management and agroforestry have also contributed to improved sustainability, while meeting increased demands for food, fiber, and livestock production[9,13–15].

While Earth's climate system is unequivocally changing[16,17], predicting the rate and magnitude of associated changes in terrestrial systems is a major unresolved challenge for evaluating coupled human-environmental impacts[18,19]. Many African communities, for example, rely on forests, woodlands and savannas for timber production and energy (fuelwood and charcoal), food (fruits, nuts, and animal rangeland), traditional medicines, and other crucial resources. Depending on the context, these land uses can enhance or reduce woody biomass[9,20]. Emissions from land-use (0.32 ± 0.05 Pg C yr^{-1}) and fire (1.03 ± 0.22 Pg C yr^{-1}), while highly variable through both space and time, are significant carbon sources[7,8]. Land use, land-use change, and fire behavior are therefore central components of global change and carbon dynamics, as the risk of land degradation from climate change and anthropogenic pressures has never been greater[21–23].

Here, we present a novel approach to deriving continental-scale estimates of above ground woody biomass by characterizing the climatic, topo-edaphic, and socioeconomic conditions that have shaped the distribution of tree and shrub biomass across the African landscape and evaluate ecosystem response to multiple scenarios of disturbance. We explore the spatial patterns of contemporary woody vegetation using a new Earth observation (EO) dataset[24] that integrates optical phenological metrics, microwave and LiDAR, providing an improved characterization of woody cover and biomass, particularly in the open and low-stature savannas of sub-Saharan Africa (Methods). We use a data-driven, machine-learning-based approach to examine how climate, human pressures, fire, and topo-edaphic conditions impact biomass variability across the continent (Extended Data Fig. 1). Ecosystem response to climate change is evaluated using the fitted relationships to empirically project and quantify the potential distribution of biomass for the end of the 21st century. Contemporary and future climate conditions are represented with long-term mean-annual aridity (calculated as 1 – [precipitation/potential evapotranspiration]), derived from a 27-model ensemble (Supplementary Table 1) participating in the fifth phase of the Coupled Model Inter-comparison Project (CMIP5). Two climate-forcings (representative concentration pathways, RCP 4.5 and RCP 8.5) are used to investigate ecosystem response under a broad range of potential climate-change scenarios for the end of this century. We also evaluate ecosystem

response to assumptions regarding future population growth and socio-climatic driven changes in fire behavior.

Biomass prediction and evaluation

Comparing our biomass predictions with the satellite-derived estimates yields excellent agreement (Supplementary Table 2) and confirms broad geographic expectations, with the density of woody biomass greatest near the equator and generally declining with latitude, but with considerable spatial variability associated with regional-scale topo-edaphic heterogeneity and climate (Fig. 1). Validation against an independent test set (N = 18,320) indicates that our model explains *ca.* 89% of the variation in tree and shrub biomass with low bias and low variance (Supplementary Table 3). Further comparison reveals that our biomass predictions are consistently at the low end of the range of previously reported estimates (Supplementary Table 4). However, it is important to note that models from previous studies[25–28] were trained exclusively with data sampled from forested regions, whereas the satellite-derived estimates[24] used to train our model better characterize the open and low-stature canopies of the savannas and drylands of Africa, which are underrepresented in most woody-cover datasets despite covering more than half of the African continent[29].

Evaluation of the conditional distributions from our covariate set indicates that climate has the largest effect on the contemporary distribution of woody biomass, which decreases as aridity[12], fire[31], human pressures[32], and sand content[33] increase (Fig. 2). Aridity alone explains 75% of the variance across sub-Saharan Africa, where mean biomass density is greatest in humid (103.9 ± 87.6 Mg ha^{-1}, mean ± 1 standard deviation) and dry sub-humid (27.1 ± 21.2 Mg ha^{-1}) regions, including the moist tropics (185.9 ± 69 Mg ha^{-1}), eastern Madagascar (94.9 ± 63 Mg ha^{-1}), and East African Highlands (44.2 ± 39 Mg ha^{-1}). Conversely, biomass density is lowest in Africa's hyper-arid ($9e^{-3}$ ± 0.1 Mg ha^{-1}), arid (1.3 ± 2.3 Mg ha^{-1}), and semi-arid regions (8.8 ± 9.9 Mg ha^{-1}). In the water-limited, drought-seasonal savannas of the Sahel, mean biomass density ranges from 1.0 ± 2 Mg ha^{-1} in the west to 2.4 ± 3 Mg ha^{-1} in the east.

Fire is most extensive in semi-arid and dry sub-humid climate zones (Methods 2.4). Indeed, nearly half (45%) of the land area impacted by fire each year occurs in the Sudanian savannas—where mean biomass density ranges from 21.5 ± 24 Mg ha^{-1} in the west to 44.6 ± 42.8 Mg ha^{-1} in the east. Human pressures also have an overall negative effect on biomass density in our model (Fig. 2). However, the relationship between humans and woody biomass is nuanced. In remote areas where anthropogenic disturbance is low (e.g., index scores of *ca.* 10 or less), biomass declines nearly linearly in response to increasing anthropogenic pressures. The strength of the effect weakens and even begins to increase as human pressures increase further, perhaps reflecting human promotion of forest cover in and around settlements[20]. For example, conservation and restoration efforts such as the 'shelterbelts' in Nigeria, Mali and Burkina Faso, 'green belts' spanning the Sahel, and agroforestry have had a profound impact on woody-vegetation recovery in recent decades[9,34,35]. However, the human footprint relationship is characterized by a large degree of uncertainty, especially in areas with relatively moderate index scores (e.g., between 20

and 35) and further analysis is required to fully tease apart the nuanced relationship between woody biomass and anthropogenic disturbance.

Aridification yields a biomass deficit

Our end-of-the-century projections suggest that woody biomass respectively declines by 0.5 – 2.5% in response to climate changes under RCP 4.5 and RCP 8.5, representing a biomass deficit of *ca*. 0.4 – 2.1 Pg relative to our predictions for the contemporary (i.e., baseline) period. While the overall spatial patterns of change are similar under both climate scenarios, the direction and magnitude of the response are amplified under RCP 8.5 (Fig. 3). Broadly speaking, woody vegetation tends to decline across most of West, Central, and Southern Africa in response to hotter and drier climate conditions. The already dry landscape of southern Africa is expected to become more arid, particularly in South Africa, where aridity under RCP 8.5 is expected increase by 6 – 10% relative to the baseline period (See Methods 2.2).

Per unit area, the largest responses occur in the Cape and Namib desert regions, with the density of woody vegetation declining by *ca*. 15 – 33% depending on the scenario. However, these regions contribute a small fraction to the bottom line of Africa's biomass budget, and therefore represent a relatively small fraction of the future deficit. In regard to biomass stock (and thus carbon storage), the largest projected deficits in response to climate changes occur in the central-mesic region and the West Sudanian Savannas, where woody biomass declines by *ca*. 0.3 – 2.1 Pg (Fig. 3). Under RCP 4.5, however, the magnitude of loss is much lower (−0.01 Pg), and the deficit is largely offset by growth in the Eastern Sahel (+0.01 Pg). In West Africa, biomass deficits under RCP 4.5 emerge primarily in the western-most extent of the mesic Sudanian and Guinean savanna regions (e.g., southern Senegal, Guinea, Guinea-Bissau, and southern Mali). However, a much larger portion of West Africa is expected to incur deficits under RCP 8.5, with projected losses expanding further east and south across much of coastal West Africa (Fig. 2b).

Most of the projected biomass growth occurs throughout East Africa, where mean biomass density (Mg ha^{-1}) increases by *ca*. 21 – 78% in response to warmer and wetter climate conditions. The largest potential increase for carbon storage occurs in the Horn of Africa (0.5 – 1.2 Pg), followed by the Rift Valley region (0.4 – 0.5 Pg), and the Highlands of East Africa (0.2 – 0.3 Pg). Although the density of woody vegetation has a relatively strong response to increasingly humid conditions across much of the semi-arid landscape of the Central and Eastern Sahel (e.g., northeastern Mali, Niger and Chad; Extended Data Fig. 2), productivity will likely remain constrained by mean-annual rainfall. The carbon-storage potential of the Sahel is therefore expected to remain relatively low, with biomass increasing by *ca*. 0.01 – 0.04 Pg.

Fire dynamics have mixed effects

While Africa accounts for the majority of Earth's fire-derived carbon emissions (52%)[7], recent research indicates that burned-area extent has declined across sub-Saharan Africa[36,37]. Evaluation of our burned-area projections, driven by changes in climate and

human pressures, suggest that this trend may continue through the end of the century, particularly in the semi-arid and dry sub-humid regions of Africa, where projections of burned-area extent decline by 2 – 15% in response to the considered forcing scenarios. However, our results for the larger Sub-Saharan Africa region suggest that Africa's already large contribution to global fire-derived carbon emissions may actually increase in the coming decades in response to aridification and increased fuel and flammability in humid regions, where the potential loss in woody biomass is relatively large.

At the continental scale, the impacts of fire on above ground woody biomass have virtually no effect under RCP 4.5, as regional gains and losses offset each other (Supplementary Table 5). Under RCP 8.5, however, changing fire regimes appear to reduce Africa's total woody biomass by an additional 1.7 Pg. The major fire-induced losses in carbon are attributed to reduced precipitation and higher evaporative demand in the moist tropics, where burned area is projected to increase and biomass density is one to two orders of magnitude larger than biomass density in other biophysical regions. Relatively large deficits in response to burned-area projections under RCP 8.5 are also expected to occur in eastern Madagascar (−0.5 Pg), as well as in East (−0.2 Pg) and West Sudanaian savannas (−0.2 Pg). Conversely, burned area is expected to decrease across large portions of East Africa, which has a small but positive effect on total biomass in the East African Highlands, the Rift Valley, and the Horn of Africa, presumably due to reduced fuels flammability in response to an increasingly humid climate. A reduction in burned area in the East Sudanian Savannas offsets the negative effects of climate changes under RCP 4.5, resulting in a small increase relative to the baseline period.

Anthropogenic pressures exacerbate climate-driven deficit

Our findings suggest that human pressures not only exacerbate the climate-driven deficits that are projected for much of West, Central, and Southern Africa, but also abate much of the growth response expected to occur across large portions of East Africa. Depending on the forcing scenario, above ground woody biomass is expected to decline by 4 – 8% in response to the compounding effects of changes in climate, fire disturbance, and human pressures —representing a deficit of *ca.* 3.4 – 6.7 Pg relative to our predictions for the baseline period. The largest deficits under these assumptions occur in the moist tropical and central mesic regions, where biomass declines by *ca.* 1.2 – 2.8 Pg. In the East African Highlands, where biomass increases in response climate changes under both forcing scenarios, human pressures offset the growth response under RCP 4.5, resulting in a small deficit (Figure 3). This trend also occurs under RCP 8.5; however, the effects of climate changes outweigh those from human pressures because the growth response is much larger under the high emissions scenario.

Regional differences regarding the direction and magnitude of change in response to human pressures largely depend on projections regarding local population and economic development assumptions under SSP2[38]—the "middle of the road" Shared Socioeconomic Pathways scenario (See Methods 2.3 and Extended Data Fig. 3). The largest relative change occurs in Niger (Fig. 5), where human pressures increase by 50%, followed by Liberia (31%), Chad (28%), and Egypt (28%). Conversely, index scores increase by just 1% in

Lesotho, and are expected to decrease in South Africa (−0.6%) and Zimbabwe (−5%), presumably due to regional differences in birth rates and/or emigration. While woody biomass has a small, positive response to the aforementioned demographic trends in South Africa and Zimbabwe, the effects of aridification are much stronger, resulting in an overall deficit under these assumptions.

Discussion

The compounding effects of climate change, regional increases in human pressures due to population and socioeconomic growth, and increased fire disturbance in heavily vegetated regions are expected reduce woody biomass by 4 – 8% across sub-Saharan Africa, representing a deficit of *ca.* 3.4 – 6.7 Pg relative to our contemporary estimates. Distinct spatial patterns of change are similar between the considered climate-forcing scenarios, but the trends are amplified under RCP 8.5. Our projections suggest that above-ground woody carbon storage declines across most of West, Central, and Southern Africa in response to increasingly arid conditions associated with climate changes. A small portion of the projected deficit is expected to be offset by growth in East Africa and other regions in response to warmer and wetter climate conditions.

Our evaluation of Anthropocene risks is enabled by integrating Representative Concentration Pathways with Shared-Socioeconomic Pathways—which were developed to provide a framework for a new generation of climate change research[39]. Anthropogenic pressures generally exacerbate the climate-driven deficit; however, considerable scope exists to determine how natural systems respond to socioeconomic transformation—such as land-use change and/or community-based restoration efforts—and if non-linearity or tipping points exist where anthropogenic pressures lead to accelerated impacts. Our assessment of anthropogenic pressures via the human-footprint index circumvents the limitations of relying solely on remote sensing, which has difficulty in detecting low intensity pressures[40] and often confounds natural and anthropogenic land-cover patterns in arid and patchy environments[41]. This approach is, however, subject to three primary constraints. First, these data do not fully account for all human activities, such as invasive species and pollution[32] or conservation and restoration efforts. Second, we model future human pressures from socio-economic narratives of population dynamics only, leaving infrastructure, energy networks, and other data static. Third, we use the Shared Socioeconomic Pathways ‘middle of the road’ assumptions (SSP2) regarding population dynamics[38,39]. Therefore, we consider our projection of anthropogenic pressures to be conservative, as transportation networks, built environments, and agriculture will presumably expand with socioeconomic growth.

While our models do not incorporate mechanistic relationships or biogeochemical feedbacks that could alter the climate-driven trends, our results are generally consistent with those reported by Martens and colleagues[42], who used an adaptive Dynamic Global Vegetation Model (aDGVM) to quantify ecosystem response to climate forcings under RCP 4.5 and RCP 8.5. The authors reported that woody vegetation changed between −8 to 11% under RCP 4.5, and by −22 to −6% under RCP 8.5 when CO_2 enrichment was omitted. When the CO_2 effect was included, the authors reported that aboveground vegetation changed between 18% to 43% (RCP4.5) and 37% to 61% (RCP8.5), and that this

change was primarily associated with woody encroachment into grasslands and increased woody cover in savannas. However, some research suggests that general circulation and Earth system models may be overly sensitive to CO_2 enrichment[43] and that the CO_2 effect is weakened when moisture constraints are strong[44]. There is also evidence to suggest that CO_2 enrichment may cause woody plants to complete their lifecycles faster[45], therefore increasing biomass turnover and offsetting carbon sequestered in response to CO_2 enrichment[46]. Our approach is deliberately data-driven and empirical, acknowledging that although our models capture the socio-environmental components that explain much of the variability in the contemporary distribution of woody biomass, empirical projections may not fully capture the mechanistic relationships leading to the observed patterns of change. Indeed, the scenarios presented here are intended to provide insight into the multidimensional aspects of global change.

Climate change—coupled with population growth, economic development and land-use change—will inevitably lead to long-term and widespread changes in vegetation structure and carbon storage in Africa and other continents. Our understanding of these trends—and the appropriate policy and land-management decisions needed to promote economic wellbeing and carbon sequestration—should be guided by research that not only examines the implications of climate-changes, but how economic development, demographic trends, and land management is likely to change over the next century. This information is essential to refine our understanding of how Anthropocene risks might impact coupled biophysical and social systems in the coming years. This is especially important for promoting and ensuring sustainable land use for the African communities that rely on local forests, woodlands, and savannas for energy, food, livestock grazing, traditional medicines, and other essential resources.

Data availability

The datasets used for this analysis can be accessed as described below.

1. Woody cover and biomass data[24] are available GeoTiff files from the Oak Ridge National Laboratory (ORNL) Distributed Active Archive Center (DAAC; https://doi.org/10.3334/ORNLDAAC/1777).
2. Aridity data were provided by Feng and Fu[12].
3. The Human Footprint map[32] is available as a GeoTiff file from Dryad (https://doi.org/10.5061/dryad.052q5).
4. Future projections of human population density based on Shared Socioeconomic Pathways[38] are available as GeoTiff files from the Socioeconomic Data and Application Center (SEDAC; https://doi.org/10.7927/m30p-j498).
5. Contemporary estimates of burned area are available as GeoTiff and were acquired from Kahiu and Hanan[31].
6. HYSOGs[47] data are available as GeoTiff from the ORNL DAAC (https://doi.org/10.3334/ORNLDAAC/1566).

7. Shuttle Radar Topography Mission (SRTM) elevation data were acquired from the United States Geological Survey (USGS) Earth Explorer (https://earthexplorer.usgs.gov/).

8. Biophysical regions were derived from The Nature Conservancy Terrestrial Ecoregions and are provided as GIS shapefiles (http://maps.tnc.org/gis_data.html).

9. Biomass prediction maps[48] and R code[49] are available from Figshare.

Methods

1. Overview of methods

We developed predictive relationships between satellite-derived estimates of woody biomass[24] and socio-environmental covariates in R 3.4.4[50] with the random forest package[51]. The random forest algorithm[52] was chosen as it allows for non-linear, non-monotonic relationships between the target property and multiple covariates. Predictive relationships were modeled from a sample of the satellite-derived woody biomass estimates, which was achieved by extracting grid-cell attributes from our covariate set and satellite-derived woody biomass estimates at 100,000 randomly generated point locations. Missing values were removed, leaving 99,471 rows in our modeling matrix. All random forest (RF) models were developed on a training set (80%) and model performance was assessed with a held-out validation set (20%). Training (n =79,576) and validation (n =19,894) sets were determined by splitting the data frame at random, an optimal *mtry* value of 4 was identified with the *tuneRF* function, and 1,000 individual trees comprised the forest. The two sample Kolmogorov-Smirnov test was conducted to verify that the distribution of woody biomass was similar between training and validation sets[53].

2. Socio-environmental data

The spatial distribution of woody biomass was modeled with key socio-environmental drivers, including aridity[12], anthropogenic disturbance[32], burned area estimates[31], elevation[54], and hydrologic soil groups[33,47] (Extended Data Fig. 1). All data were projected to a common coordinate system (sinusoidal equal-area) and, if necessary, re-sampled to match the spatial resolution of our woody biomass product (1 km^{-2}). Bilinear interpolation and nearest neighbor were used to resample continuous and categorical data, respectively.

2.1 Woody biomass—Satellite-derived estimates of woody biomass were provided by Hanan et al.[24] at 1 km^2 resolution for sub-Saharan Africa (Extended Data Fig. 4). These estimates are a product of data integration, which was achieved by applying allometric equations to relate biomass with canopy cover and canopy height. Canopy cover estimates were produced at 1 km^2 resolution by combining phenological metrics from MODIS with Quick-Scatterometer ku-band microwave retrievals. This product was chosen to represent canopy cover as it provides an improved assessment of low stature systems by accounting for vegetation less than 5 m in height, which occupy a considerable fraction of the African landscape but remain under-represented in widely-used tree-cover datasets due to mapping challenges presented by their complex landscapes, and the underestimation of

woody plants by methods that exclude short stature trees and shrubs[29]. Canopy height was estimated by Simard and colleagues[55] from light detection and ranging (LiDAR) at 1 km^2 resolution. Biomass estimates were derived by relating canopy cover to canopy height with an allometric equation derived from the globallometree.org database[56].

2.2 Aridity—Global coverage of the aridity-index was provided as a 27-model ensemble mean by Feng and Fu[12] (Supplementary Table 1). The aridity index (AI = precipitation / potential evapotranspiration) was calculated using the Penman-Monteith method, which accounts for the effects of surface-air temperature, humidity, solar radiation, and wind speed. These data were temporally averaged over the CMIP5 historical forcing's (1980 to 2005) to model satellite-derived estimates of existing woody biomass. Aridity was then calculated as 1 – AI so that increasingly larger values correspond to increasingly drier conditions. Ecosystem response to climate change (CMIP5 aridity projections) was modeled under representative concentration pathways (RCP) 4.5 and RCP 8.5. These RCPs were chosen to represent a broad range of potential climate change scenarios.

2.3 Human footprint—Following Venter and colleagues[32], we adopted the human-footprint methodology[57] to project human pressures in response to population growth assumptions[38] for end of the 21st century. Contemporary human pressures were related to satellite-derived estimates of woody biomass via the 2009 'Human Footprint' map[32], which was developed through cumulative pressure mapping by integrating datasets of built environments, population density, electric infrastructure, croplands, pasture lands, roads, railways, and navigable waterways. Venter and colleagues[32] developed the Human Footprint index by first standardizing each dataset on a scale of 0 to 10 to obtain individual pressure scores for each dataset. Anthropogenic 'pressure scores' are then summarized into a single dataset to produce the Human Footprint index (Figure 3a). Low scores (e.g., 0 to 5) correspond to areas that that receive little or no pressure from human activities. Conversely, highly impacted areas (e.g., large cities) are assigned larger scores, with a maximum score of 50.

To assess biomass dynamics in response to end-of-century human pressures, we produced a future Human Footprint map (Figure 3b) by calculating the population pressure score for 2100. Projected population density was derived from the Global Population Projection Grids Based on Shared Socioeconomic Pathways (SSPs)[38]. We choose SSP2, which represents a conservative ('middle of the road') scenario regarding spatiotemporal patterns of population, urbanization, and development demographics. Following the human footprint methodology, a pressure score of 10 was assigned to all grid cells with 1,000 or more people km^{-2}. Population pressure scores for the remaining grid cells were logarithmically scaled (Eq. 1).

$$Pressure\,score = 3.33 \times \log(population\,density + 1) \quad (1)$$

To obtain an index score for the future human footprint, we summarized the pressures scores provided by Venter and colleagues[32], substituting the 2009 population pressure score with the SSP2 population pressure score. While future projections of other anthropogenic activities (e.g., agricultural expansion, transportation, built environments, etc.) have not yet been developed, they are correlated with the increase in human population density. Thus, our

future human footprint map is considered a conservative estimate of human pressures for 2100.

2.4 Burned area—Long-term (2003 to 2015) mean-annual burned area was provided from Kahui and Hanan[31]. These data were produced from Earth observations of monthly burned area estimates obtained from the Global Fire Emissions Database (GFED) with a spatial resolution of 0.25° (Extended Data Fig. 1). While most African fires are attributed to land use and management, climate strongly influences fire intensity, severity, and wildfire spread. We therefore model contemporary burned area as a function of climate (i.e. aridity), dry season precipitation, anthropogenic pressures as indexed by the human footprint, and elevation (Extended Data Fig. 1). Specifically, we used long-term mean-annual aridity and dry-season precipitation, elevation, and the Human Footprint map. The same set of randomly generated point locations described in the methods overview were used to extract the grid-cell attribute information from the aforementioned covariates. Model evaluation with the independent validation set (N = 20%) indicates that our random forest model was able to explain 72% of burned-area variation, corresponding to a RMSE of 8.8%. Evaluation of accumulated local effects, obtained from the Interpretable Machine Learning package[58], indicates that aridity is the most important predictor of burned area, followed by dry-season precipitation, elevation, and human pressures. Burned area projections for the end of the 21st century (2071 to 2100) were projected in response to changes in human pressures, mean-annual precipitation and dry-season precipitation.

2.5 Topo-edaphic properties—Hydrologic soil groups (0 – 100 cm) were obtained from the HYSOGs250m dataset[47], which integrates data pertaining to soil texture classes, depth to bedrock, and depth to water table. Three arc-second, gap-filled Shuttle Radar Topography Mission (SRTM) elevation data was acquired from earthexplorer.usgs.gov. We assume that the aforementioned topo-edaphic properties (Extended Data Fig. 1) will not change substantially by 2100, and were therefore treated as constants in our model.

3. Model evaluation

Model evaluation and data analysis was performed with the tidyverse package[59], and figures were produced using raster[60], rasterVis[61], ggplot2[62], colorspace[63], RColorBrewer[64], gridExtra[65], iml[58], and sf[66] packages. Data-model fit was evaluated with the coefficient of determination (R^2, equation 2), root mean squared error (RMSE, equation 3), residual prediction deviation (RPD, equation 4), and the ratio of performance to interquartile distance (RPIQ, equation 5).

$$R^2 = 1 - \frac{\sum_{i=1}^{n} (y_i - \hat{y}_i)^2}{\sum_{i=1}^{n} (y_i - \bar{y})^2}. \quad (2)$$

$$RMSE = \sqrt{\frac{1}{n} \sum_{i=1}^{n} (\hat{y}_i - y_i)^2}. \quad (3)$$

$$RPD = \frac{SD}{RMSE\sqrt{n/(n-1)}}. \quad (4)$$

$$RPIQ = \frac{IQ}{RMSE}. \quad (5)$$

where, $\widehat{y_i}$ are the model predicted values, y_i are the observed values, n is the number of predicted or observed values in the held-out dataset (testing) with $i = 1, 2, \ldots, n$, SD is the standard deviation of the testing set, $RMSE$ is the root mean square error, and IQ is the interquartile range.

Extended Data

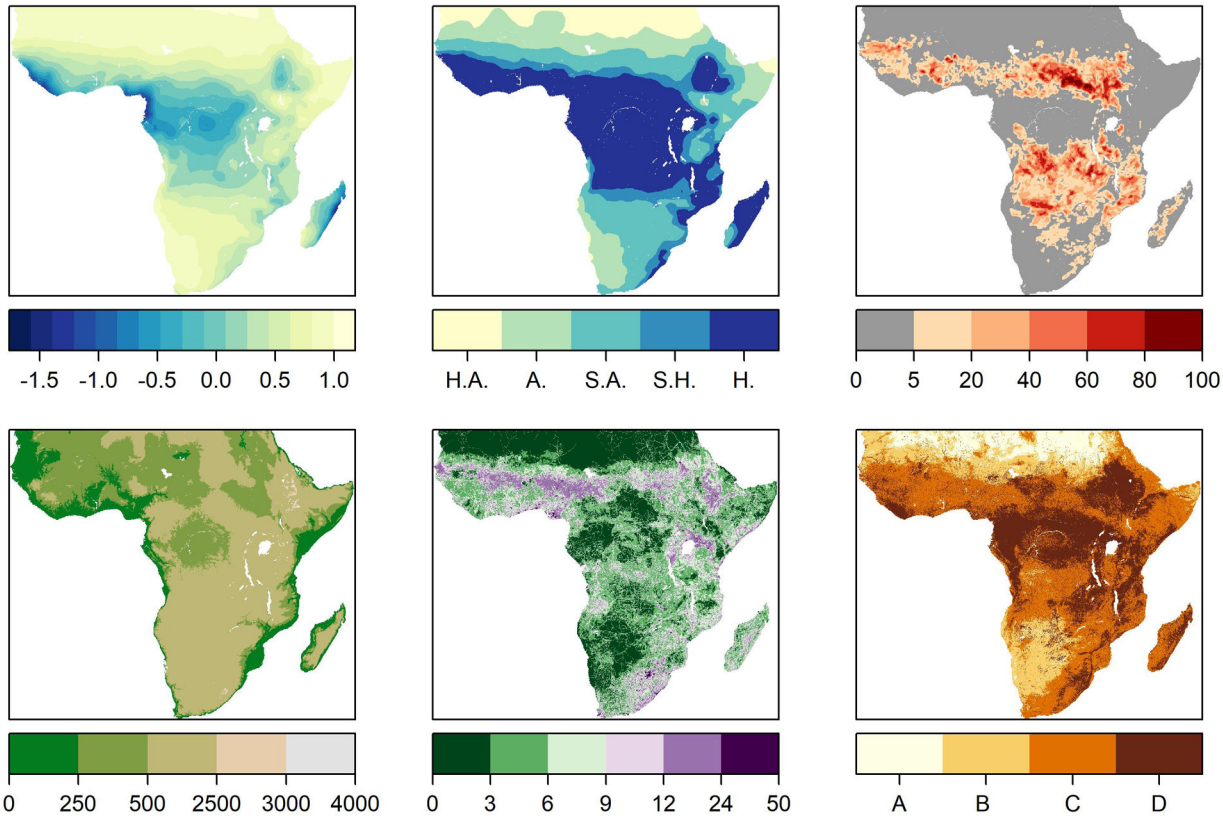

Extended Data Fig. 1. Socio-environmental data.

a) Long-term mean-annual aridity based on the historical data[12] (1981 – 2010) and **b)** climate zones, with H.A., hyper-arid; A., arid; S.A., semi-arid; S.H., Sub-humid; H., humid. **c)** Satellite-derived estimates of mean annual (2003 – 2015) burned-area (%)[31]. **d)** Digital elevation model[52]. **e)** The contemporary human footprint index[32]. **f)** Hydrologic soil groups[33], with A corresponds to low runoff-potential soils (e.g., sands); B, moderately low runoff-potential; C, moderately high runoff-potential; D, high runoff-potential (e.g., clays).

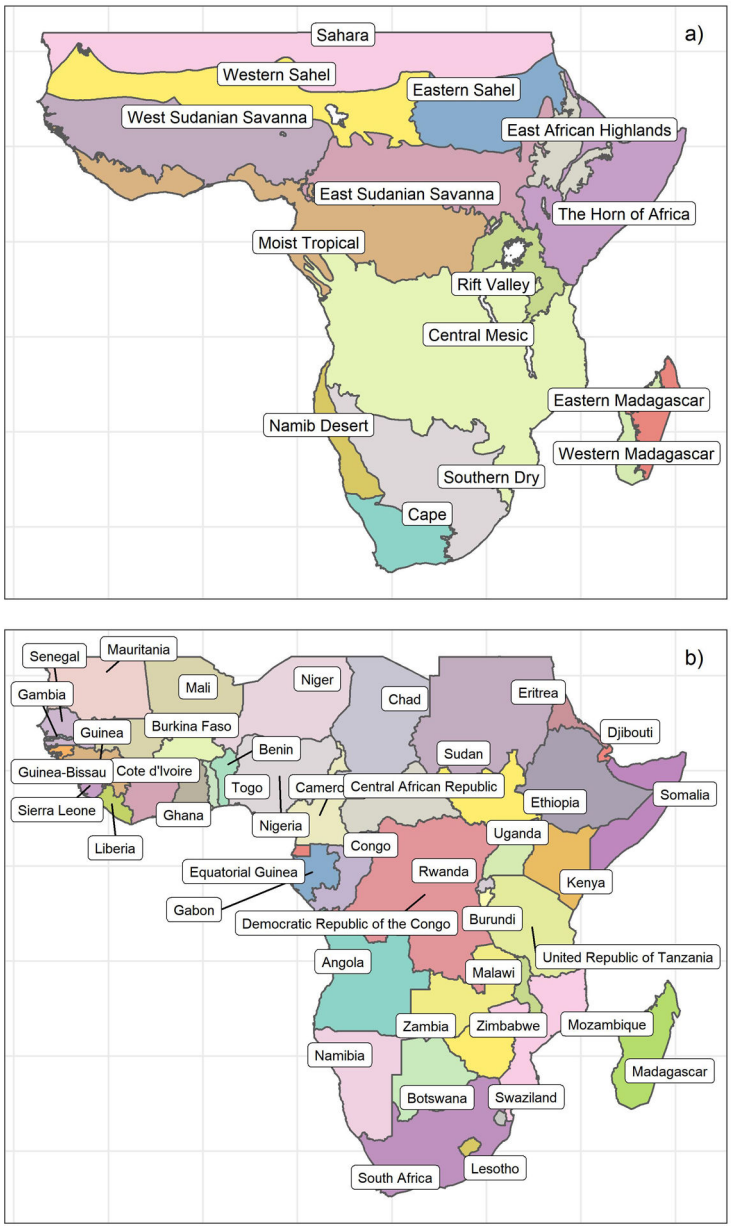

Extended Data Fig. 2. Biophysical regions and countries of sub-Saharan Africa.

a) Biophysical regions were derived by aggregating The Nature Conservancy Terrestrial Ecosystems[30] into broader classes. **b)** Country borders were mapped using the R sf[64] package.

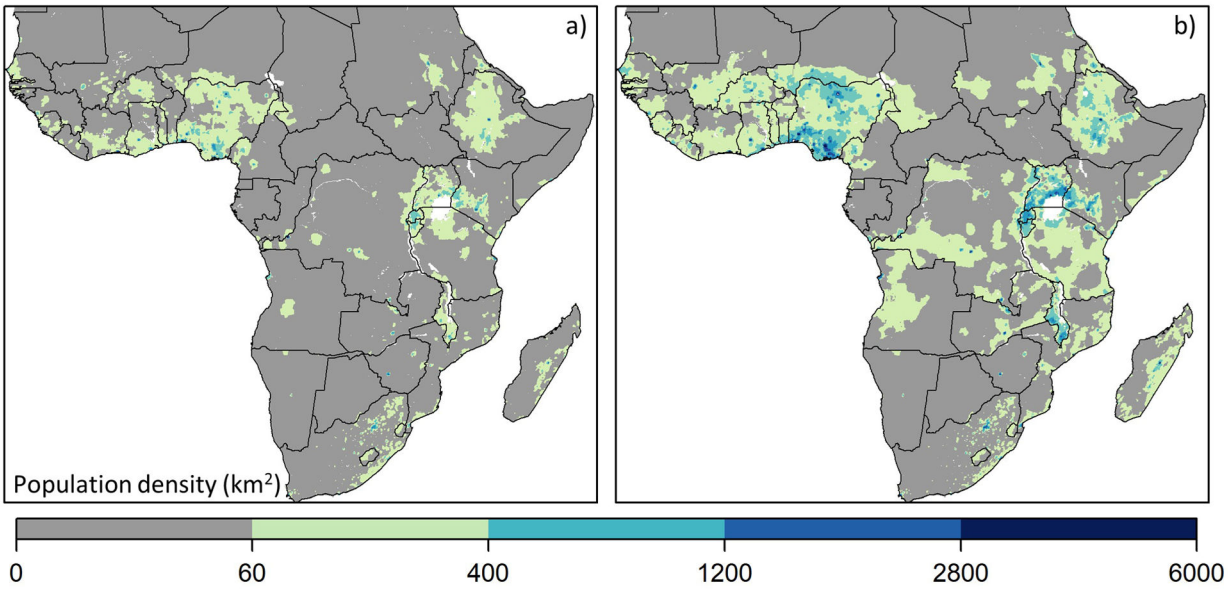

Extended Data Fig. 3. Human population density.

a), Population density (people per km^{-2}) for 2010 and b) projected population density for 2100 under the “middle of the road” Shared Socioeconomic Pathways (SSP2)[38].

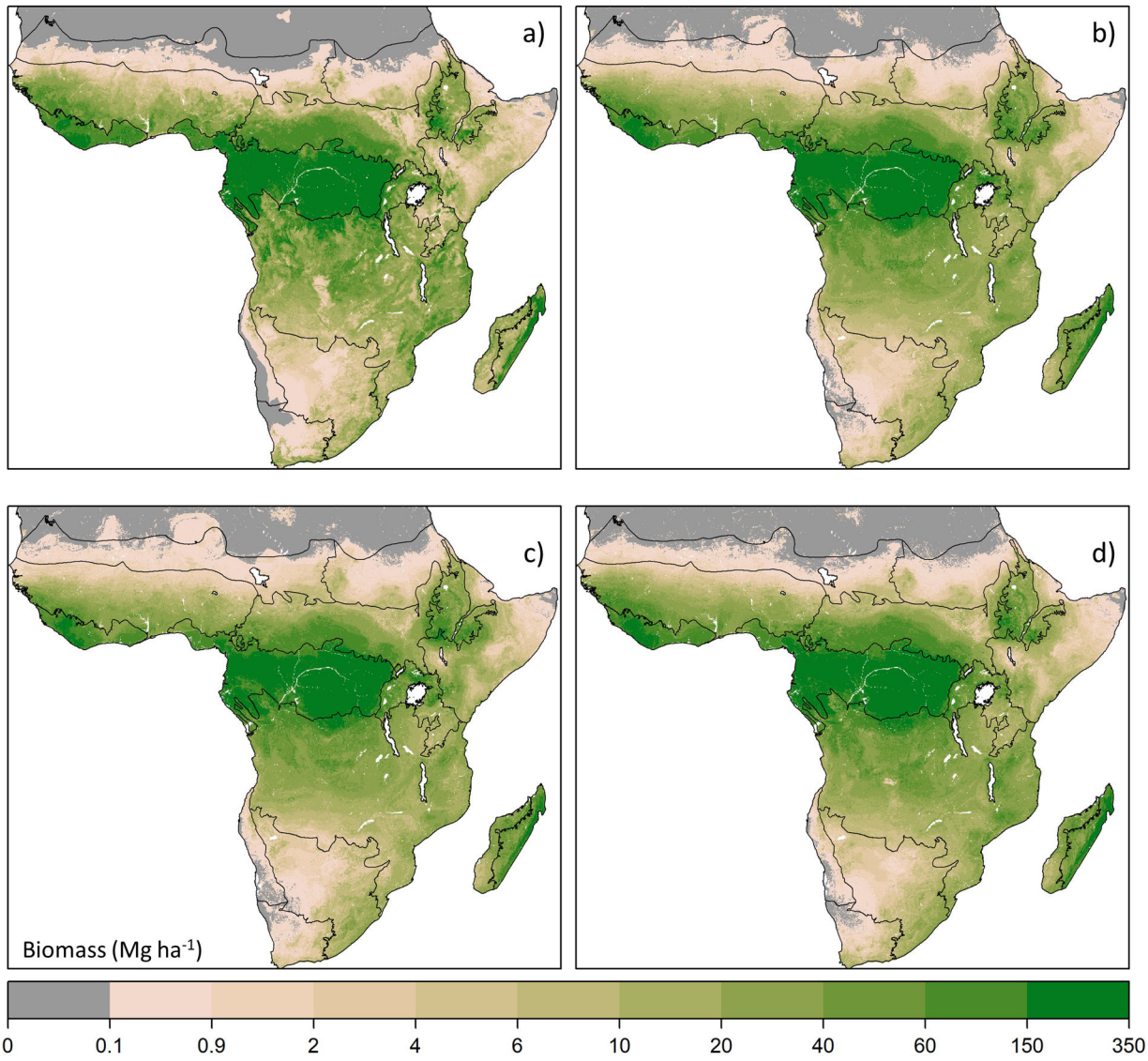

Extended Data Fig. 4. Above-ground woody biomass (Mg ha^{-1})

a), Satellite-derived estimates of above-ground woody biomass[24]. b), Predicted above-ground biomass representing the baseline (i.e., contemporary) estimates. c), End of century empirical projection of woody biomass in response to RCP 4.5 and assumptions regarding population growth and fire regime changes. d), End of century empirical projection of woody biomass in response to RCP 8.5 and assumptions regarding population growth and fire regime changes. Data are available for download[48] as GeoTiffs.

Supplementary Material

Refer to Web version on PubMed Central for supplementary material.

Acknowledgements

This research was supported by the U.S. National Aeronautics and Space Administration (NASA) as part of the NASA Carbon Cycle Science program. Grant # NNX17AI49G, N.P.H., L.P. We thank Sanath Kumar, Brianna Lind, Haneen Omari, Caroline Toth, Paul Jacob Burch Stickel, and Robert Wojcikiewicz for their contributions to this analysis. We also thank the reviewers for their keen eyes and their critique, which has improved this article.

References

1. Davis SJ & Caldeira K Consumption-based accounting of CO2 emissions. PNAS 107, 5687–5692 (2010). [PubMed: 20212122]
2. Wiedmann TO et al. The material footprint of nations. PNAS 112, 6271–6276 (2015). [PubMed: 24003158]
3. Rogelj J et al. Paris Agreement climate proposals need a boost to keep warming well below 2 °C. Nature 534, 631–639 (2016). [PubMed: 27357792]
4. Brandt M et al. Satellite passive microwaves reveal recent climate-induced carbon losses in African drylands. Nature Ecology & Evolution 2, 827–835 (2018). [PubMed: 29632351]
5. Sankaran M et al. Determinants of woody cover in African savannas. Nature 438, 846 (2005). [PubMed: 16341012]
6. Bond WJ & Keane RE Fires, Ecological Effects of☆. In Reference Module in Life Sciences (Elsevier, 2017). doi:10.1016/B978-0-12-809633-8.02098-7.
7. Valentini R et al. A full greenhouse gases budget of Africa: synthesis, uncertainties, and vulnerabilities. Biogeosciences 11, 381–407 (2014).
8. Williams CA et al. Africa and the global carbon cycle. Carbon Balance Manag 2, 3 (2007). [PubMed: 17343752]
9. Hanan NP Agroforestry in the Sahel. Nature Geoscience 1 (2018) doi:10.1038/s41561-018-0112-x.
10. Dai A Increasing drought under global warming in observations and models. Nat. Clim. Chang 3, 52–58 (2013).
11. Zhou L et al. Widespread decline of Congo rainforest greenness in the past decade. Nature 509, 86–90 (2014). [PubMed: 24759324]
12. Feng S & Fu Q Expansion of global drylands under a warming climate. Atmospheric Chemistry and Physics 13, 10081–10094 (2013).
13. Anchang JY et al. Trends in Woody and Herbaceous Vegetation in the Savannas of West Africa. Remote Sensing 11, 576 (2019).
14. Andela N, Liu YY, Dijk A. I. J. M. van, Jeu R. A. M. de & McVicar TR Global changes in dryland vegetation dynamics (1988–2008) assessed by satellite remote sensing: comparing a new passive microwave vegetation density record with reflective greenness data. Biogeosciences 10, 6657–6676 (2013).
15. Kaptué AT, Prihodko L & Hanan NP On regreening and degradation in Sahelian watersheds. PNAS 112, 12133–12138 (2015). [PubMed: 26371296]
16. Schneider SH The Greenhouse Effect: Science and Policy. Science 243, 771–781 (1989). [PubMed: 17820424]
17. Walsh J et al. Ch. 2: Our Changing Climate. Climate Change Impacts in the United States: The Third National Climate Assessment. https://nca2014.globalchange.gov/downloads (2014) doi:10.7930/J0KW5CXT.
18. Filatova T, Polhill JG & van Ewijk S Regime shifts in coupled socio-environmental systems: Review of modelling challenges and approaches. Environmental Modelling & Software 75, 333–347 (2016).
19. Loarie SR et al. The velocity of climate change. Nature 462, 1052–1055 (2009). [PubMed: 20033047]
20. Brandt M et al. Reduction of tree cover in West African woodlands and promotion in semi-arid farmlands. Nature Geosci 11, 328–333 (2018). [PubMed: 32944066]
21. Keys PW et al. Anthropocene risk. Nat Sustain 2, 667–673 (2019).

22. Rockström J et al. A safe operating space for humanity. Nature 461, 472–475 (2009). [PubMed: 19779433]
23. Steffen W et al. Planetary boundaries: Guiding human development on a changing planet. Science 347, 1259855 (2015). [PubMed: 25592418]
24. Hanan NP, Prihodko L, Ross CW, Bucini G & Tredennick AT Gridded Estimates of Woody Cover and Biomass across Sub-Saharan Africa, 2000–2004. (ORNL Distributed Active Archive Center, 2020). doi:10.3334/ORNLDAAC/1777.
25. Bouvet A et al. An above-ground biomass map of African savannahs and woodlands at 25m resolution derived from ALOS PALSAR. Remote Sensing of Environment 206, 156–173 (2018).
26. Avitabile V et al. An integrated pan-tropical biomass map using multiple reference datasets. Glob Change Biol 22, 1406–1420 (2016).
27. Saatchi SS et al. Benchmark map of forest carbon stocks in tropical regions across three continents. PNAS 108, 9899–9904 (2011). [PubMed: 21628575]
28. Baccini A et al. Estimated carbon dioxide emissions from tropical deforestation improved by carbon-density maps. Nature Clim Change 2, 182–185 (2012).
29. Anchang JY et al. Toward Operational Mapping of Woody Canopy Cover in Tropical Savannas Using Google Earth Engine. Front. Environ. Sci 8, (2020).
30. Olson DM & Dinerstein E The Global 200: Priority Ecoregions for Global Conservation. Annals of the Missouri Botanical Garden 89, 199–224 (2002).
31. Kahiu MN & Hanan NP Fire in sub-Saharan Africa: The fuel, cure and connectivity hypothesis. Global Ecology and Biogeography (2018) doi:10.1111/geb.12753.
32. Venter O et al. Global terrestrial Human Footprint maps for 1993 and 2009. Scientific Data 3, 160067 (2016). [PubMed: 27552448]
33. Ross CW et al. HYSOGs250m, global gridded hydrologic soil groups for curve-number-based runoff modeling. Scientific Data 5, 180091 (2018). [PubMed: 29762550]
34. Lüdeke MKB, Moldenhauer O & Petschel-Held G Rural poverty driven soil degradation under climate change: the sensitivity of the disposition towards the Sahel Syndrome with respect to climate. Environmental Modeling & Assessment 4, 315–326 (1999).
35. Hansfort SL & Mertz O Challenging the Woodfuel Crisis in West African Woodlands. Hum Ecol 39, 583 (2011).
36. Andela N et al. A human-driven decline in global burned area. Science 356, 1356–1362 (2017). [PubMed: 28663495]
37. Wei F et al. Nonlinear dynamics of fires in Africa over recent decades controlled by precipitation. Global Change Biology 26, 4495–4505 (2020). [PubMed: 32445413]
38. Jones B & O'Neill BC Spatially explicit global population scenarios consistent with the Shared Socioeconomic Pathways. Environ. Res. Lett 11, 084003 (2016).
39. Riahi K et al. The Shared Socioeconomic Pathways and their energy, land use, and greenhouse gas emissions implications: An overview. Global Environmental Change 42, 153–168 (2017).
40. Potapov P et al. Mapping the World's Intact Forest Landscapes by Remote Sensing. Ecology and Society 13, (2008).
41. Herold M, Mayaux P, Woodcock CE, Baccini A & Schmullius C Some challenges in global land cover mapping: An assessment of agreement and accuracy in existing 1 km datasets. Remote Sensing of Environment 112, 2538–2556 (2008).
42. Martens C et al. Large uncertainties in future biome changes in Africa call for flexible climate adaptation strategies. Global Change Biology 27, 340–358 (2021). [PubMed: 33037718]
43. Smith WK et al. Large divergence of satellite and Earth system model estimates of global terrestrial CO_2 fertilization. Nature Climate Change 6, 306–310 (2016).
44. Reich PB, Hobbie SE & Lee TD Plant growth enhancement by elevated CO_2 eliminated by joint water and nitrogen limitation. Nature Geoscience 7, 920–924 (2014).
45. Wieder WR, Cleveland CC, Smith WK & Todd-Brown K Future productivity and carbon storage limited by terrestrial nutrient availability. Nature Geoscience 8, 441–444 (2015).
46. Körner C A matter of tree longevity. Science 355, 130–131 (2017). [PubMed: 28082545]

47. Ross CW et al. Global Hydrologic Soil Groups (HYSOGs250m) for Curve Number-Based Runoff Modeling. ORNL DAAC (2018) doi:10.3334/ORNLDAAC/1566.
48. Ross CW, Hanan NP & Prihodko L Prediction maps: Woody-biomass projections and drivers of change in sub-Saharan Africa. 754465620 Bytes (2021) doi:10.6084/M9.FIGSHARE.14150210.V2.
49. Ross CW R Code for Woody-biomass projections and drivers of change in sub-Saharan Africa. 14349 Bytes (figshare, 2021). doi:10.6084/M9.FIGSHARE.14143799.V1.
50. R Core Team. R: A Language and Environment for Statistical Computing. (R Foundation for Statistical Computing, 2019).
51. Liaw A & Wiener M Classification and Regression by randomForest. R News 2, 18–22 (2002).
52. Breiman L Random Forests. Machine Learning 45, 5–32 (2001).
53. Massey FJ The Kolmogorov-Smirnov Test for Goodness of Fit. Journal of the American Statistical Association 46, 68–78 (1951).
54. Jarvis A, Reuter HI, Nelson A & Guevara E Hole-filled SRTM for the globe Version 4. *In* CGIAR Consortium for Spatial Information (CGIAR-CSI) (2008) (2008).
55. Simard M, Pinto N, Fisher JB & Baccini A Mapping forest canopy height globally with spaceborne lidar. Journal of Geophysical Research 116, (2011).
56. Jucker T et al. Allometric equations for integrating remote sensing imagery into forest monitoring programmes. Global Change Biology 23, 177–190 (2017). [PubMed: 27381364]
57. Sanderson EW et al. The Human Footprint and the Last of the Wild. BioScience 52, 891–904 (2002).
58. Molnar C, Bischl B & Casalicchio G iml: An R package for Interpretable Machine Learning. JOSS 3, 786 (2018).
59. Wickham H tidyverse: Easily Install and Load the ‘Tidyverse’. (2017).
60. Hijmans RJ et al. raster: Geographic Data Analysis and Modeling. (2016).
61. Perpiñán O & Hijmans R rasterVis. (2018).
62. Wickham H ggplot2: Elegant Graphics for Data Analysis. (Springer-Verlag New York, 2016).
63. Zeileis A et al. colorspace: A Toolbox for Manipulating and Assessing Colors and Palettes. arXiv:1903.06490 [cs, stat] (2019).
64. Neuwirth E RColorBrewer: ColorBrewer Palettes. (2014).
65. Auguie B gridExtra: Miscellaneous Functions for ‘Grid’ Graphics. (2017).
66. Pebesma E Simple Features for R: Standardized Support for Spatial Vector Data. The R Journal 10, 439–446 (2018).

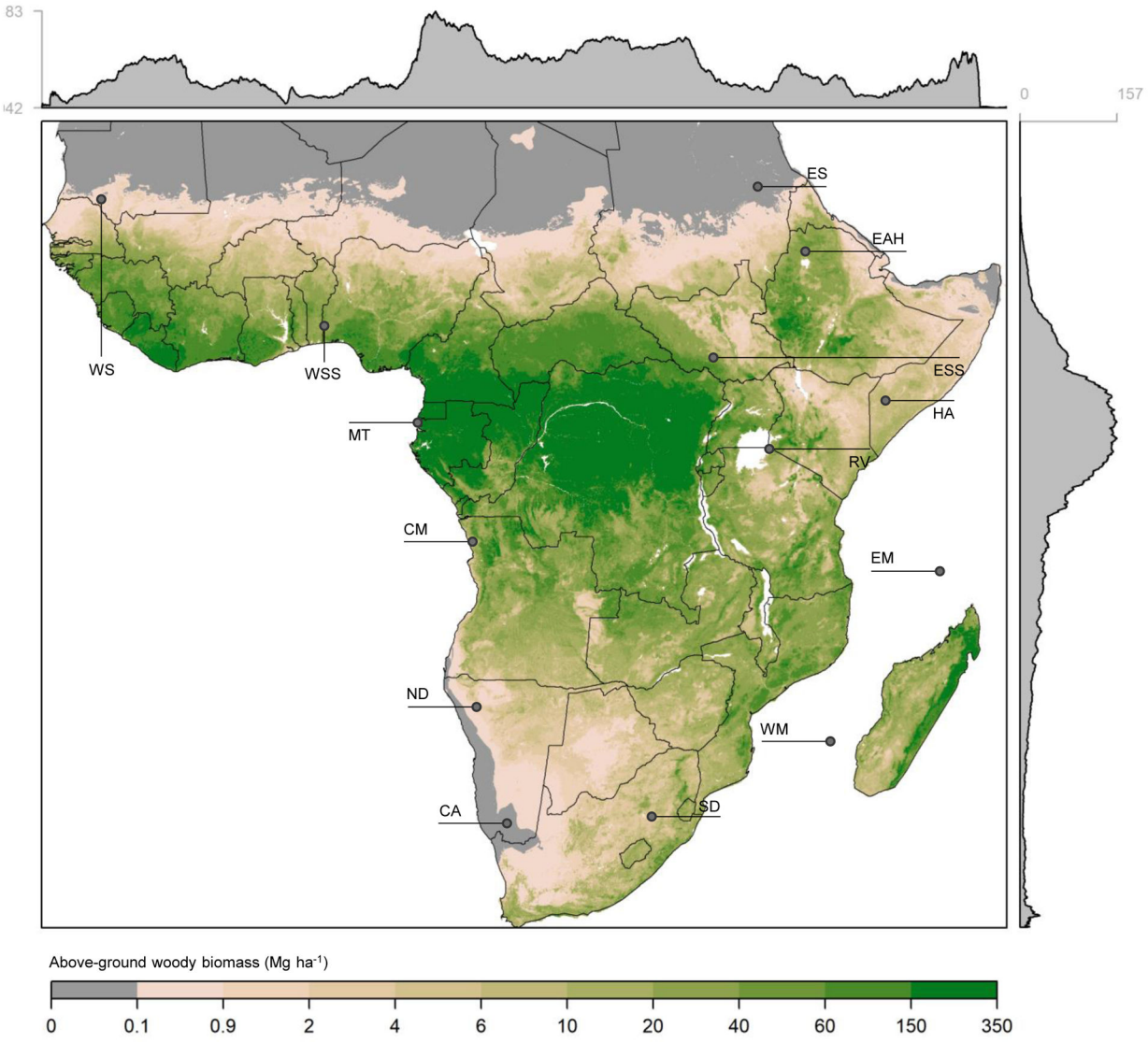

Figure 1. Satellite-derived estimates of contemporary (2005) above-ground woody biomass (Mg ha-1).

By integrating Earth-observation data from optical, microwave, and LiDAR sensors, Hanan and colleagues24 improved biomass estimates for trees and shrubs in the open and low-stature dryland and drought-seasonal savannas of sub-Saharan Africa. Marginal plots on vertical and horizontal axes correspond to woody biomass density averaged by latitude and longitude, respectively. The map overlay corresponds to ecological regions, which were derived by aggregating Terrestrial Ecosystems30 into broader classes (Extended Data Fig. 2). CA is the Cape of Africa; CM is Central Mesic; EAH is East African Highlands; EM is Eastern Madagascar; ES is Eastern Sahel; ESS is East Sudanian Savannas; HA is the Horn of Africa; MT is Moist Tropical; ND is Namib Desert; RV is Rift Valley; SD is Southern Dry; WM is Western Madagascar; WS is Western Sahel; WSS is West Sudanian Savanna.

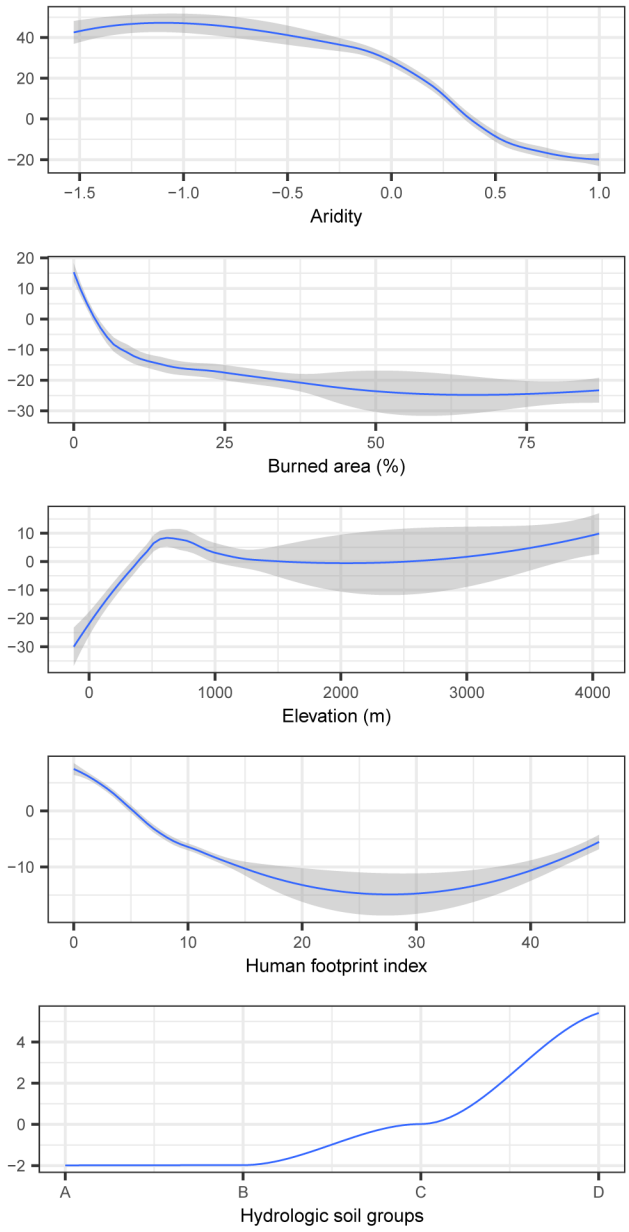

Figure 2. Sensitivity of above ground woody biomass to socio-environmental conditions.

Accumulated local effects from the fitted random forest model (n =79,576) illustrate the relationship between sub-Saharan woody biomass and socio-environmental covariates, which are ranked in order of largest (top) to smallest effect (bottom). The x-axis represents the units of the independent covariate, the y-axis represents the size of the mean effect each covariate has on woody biomass predictions, and grey shading indicates the 95% confidence interval. Aridity [calculated as 1 – (precipitation/potential evapotranspiration)] values ranging from 1.0 – 0.9, 0.9 – 0.8, 0.8 – 0.5, 0.5 – 0.35, and less than 0.35, respectively correspond to hyper-arid, arid, semi-arid, dry sub-humid, and humid regions. Hydrologic soil groups A, B, C, and D respectively correspond to soils with low run off

potential (e.g., sandy soils), moderately low, moderately high, and high runoff potential (e.g., clay soils).

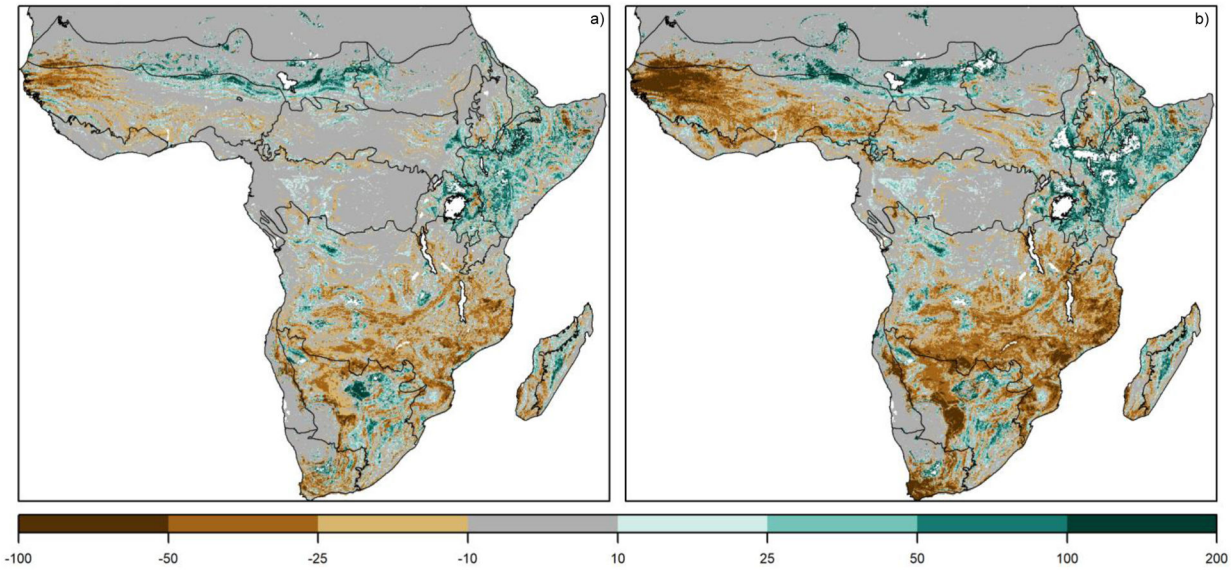

Figure 3. Projected change (%) in above ground woody biomass relative to contemporary estimates.

Each map represents the projected change (%) in the mean density of woody-biomass (1 km^{-2}) relative to the baseline period in response to projections in aridity (calculated as 1 – (precipitation/potential evapotranspiration)] under **a)** RCP 4.5) and **b)** RCP 8.5. The map overlay corresponds to biophysical regions illustrated in Fig. 1.

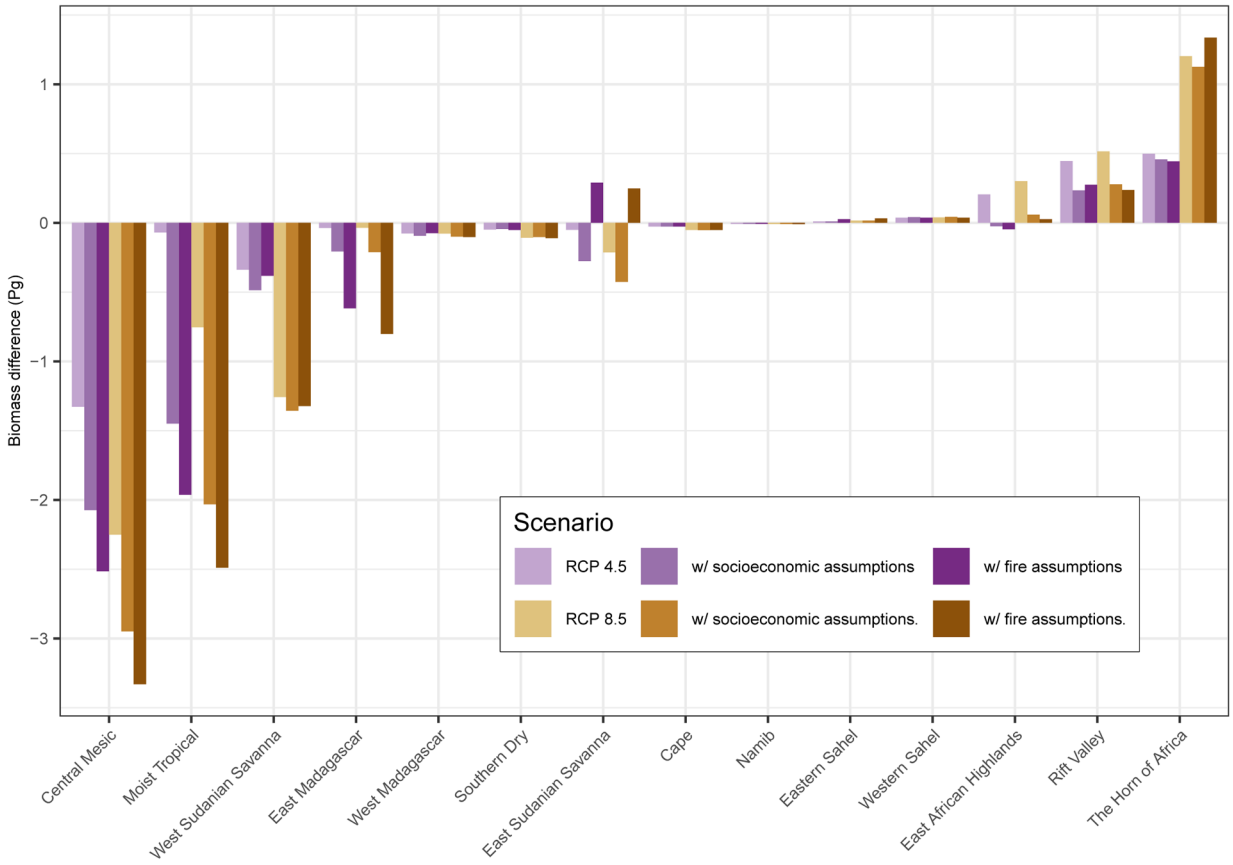

Figure 4. Projected above ground woody biomass changes in response to climate change, fire and human land use.

Projected above-ground woody biomass change (Pg) are in response to climate changes under RCP 4.5 and RCP 8.5. Also illustrated are the compounding effects of climate change and burned area, and the compounding effects of climate change, burned area, and human pressures.

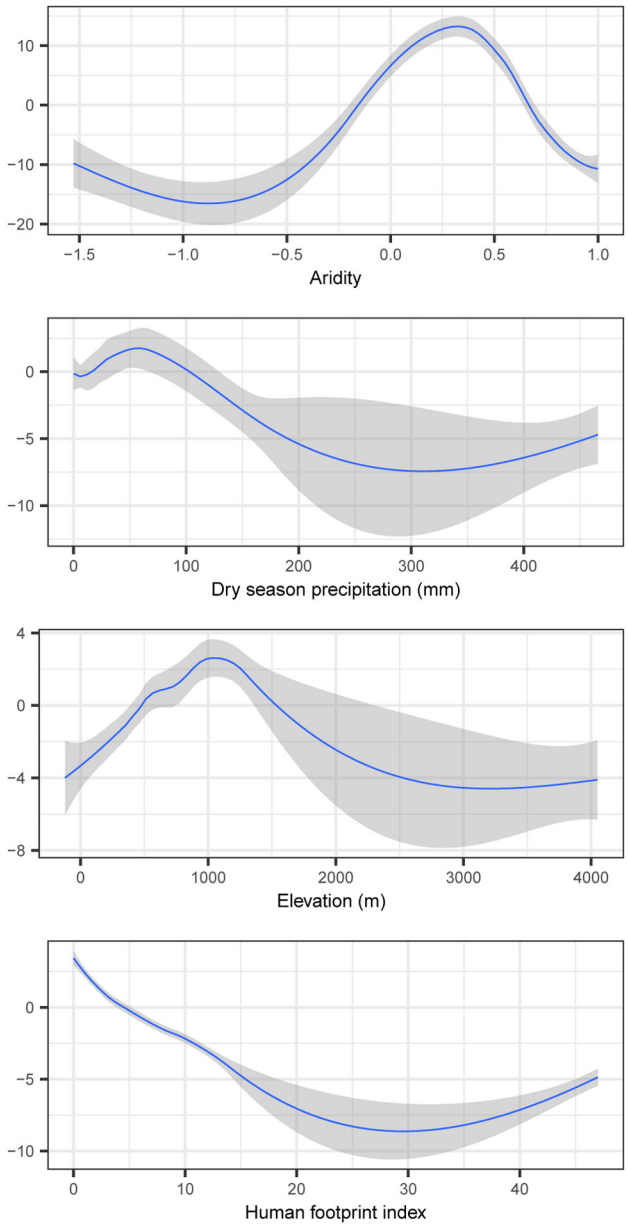

Figure 5. Sensitivity of burned area (%) to socio-environmental conditions.

Accumulated local effects from the fitted random forest model illustrate the relationship between burned-area and socio-environmental covariates in sub-Saharan Africa, which are ranked in order of highest feature importance (top) to lowest feature importance (bottom). The x-axis represents the units of the independent covariate, the y-axis represents the size of the mean effect each covariate has on woody biomass predictions, and grey shading indicates the 95% confidence interval. Note that larger human footprint values correspond to regions with higher human pressures due to anthropogenic activity.

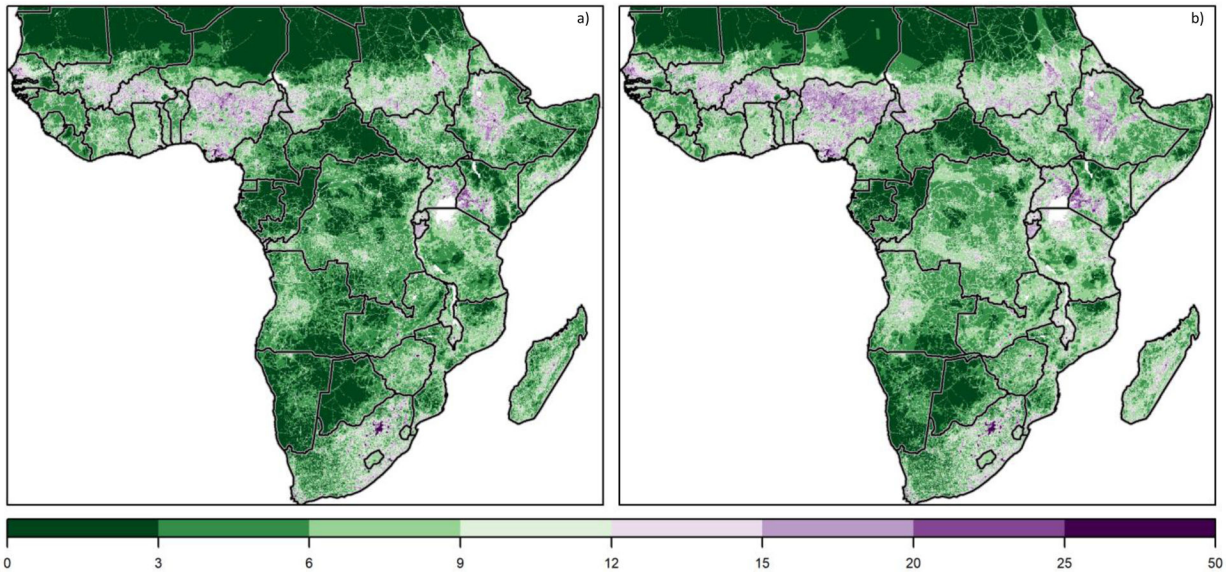

Figure 6. Anthropogenic pressure scores for sub-Saharan Africa.

a) The contemporary Human Footprint map[32] was developed through cumulative pressure mapping, integrating data regarding the built environment, population density, electric infrastructure, croplands, pasturelands, roads, railways, and navigable waterways[32]. Small index scores (e.g., 0 – 3) correspond to areas with little or no human impact, while large scores correspond to highly impacted landscapes and urban areas. **b) End of the 21st Century** human footprint index using population density projections for 2100 under the Shared Socioeconomic Pathways (SSP2) 'middle of the road' assumptions regarding population dynamics[38].